Nanoscale

ROYAL SOCIETY OF CHEMISTRY

PAPER

View Article Online
View Journal | View Issue

Cite this: *Nanoscale*, 2024, **16**, 21776

"Sergeants-and-soldiers" principle in the synthesis of intrinsically chiral Au_{13} clusters†

Katsuya Mutoh, Sonomi Kawakita, Teppei Yahagi and Takuya Nakashima *

Surface ligand modification on atomically precise metal clusters is one of the important strategies not only to stabilize monodisperse clusters, but also to derive unique optical and electronic properties. The chiral coordination of surface ligands on clusters controls the global chirality in clusters giving rise to unambiguous optical activity including circular dichroism (CD) and circularly polarized luminescence (CPL). Stereoselective synthesis of intrinsically chiral clusters has been achieved by the use of chiral ligands stabilizing one-handed clusters selectively. Herein, we investigate the effect of chiral ligand coordination on the deracemization of intrinsically chiral Au_{13} superatom clusters. The mixture of achiral bis(diphenylphosphino)ethane (DPPE) and chiral (*R*,*R*)-1,2-bis[(2-methoxyphenyl)phenylphosphino]ethane (*R*-DIPAMP) led to the formation of a mixture of $[Au_{13}(R\text{-DIPAMP})_x(DPPE)_{5-x}Cl_2]^{3+}$ clusters with varied *x*-values (*x* = 0–5). Reverse phase HPLC successfully fractionalized the mixture into solutions composed of single component Au_{13} clusters depending on the *x*-values. The separated Au_{13} clusters afforded similar optical activity to that of $[Au_{13}(R\text{-DIPAMP})_5Cl_2]^{3+}$ in the CD study regardless of *x*-values (*x* = 1–4). The DFT calculation supports that the coordination of a single DIPAM ligand is enough to bias the twisting direction in the Au_{13} superatom with dictating the tortional orientation of other four DPPE ligands. The emergence of the "sergeants-and-soldiers principle", wherein a small number of chiral ligands determine the chiral orientation of other achiral ligands, is thus demonstrated in the synthesis of intrinsically chiral Au_{13} clusters.

Received 17th September 2024,
Accepted 27th October 2024

DOI: 10.1039/d4nr03810j

rsc.li/nanoscale

Introduction

Chiral amplification phenomena have received significant attention in several research areas in chemical sciences, not only for the development of asymmetric catalysts and non-linear optical materials,[1–6] but also for seeking the origin of homochirality evolution in nature.[7–10] Effective communications among chiral/achiral building units in helical polymers and supramolecular assemblies have been investigated in detail to clarify the specific stereochemical interaction for chiral amplification.[11,12] The "Sergeants-and-soldiers principle" is one of the representative chiral amplification expressions.[13,14] An intrinsically chiral system, such as a helical polymer, built by achiral monomers usually consists of a racemic mixture of left- and right-hand ones. The introduction of a small amount of chiral monomers with a similar structure to achiral ones effectively deracemizes the system by selectively stabilizing one-handed helical polymers. The achiral monomer units obey the orientation given by the chiral ones aligning in a one-hand direction together in a helical polymer. Chirality could thus be significantly amplified by a slight chiral input as a result of strong cooperative interactions among monomers and the entire polymer, producing chiral polymers with a large helical sense excess.

Ligand-protected metal clusters have been extensively investigated in recent years owing to their unique electronic properties derived from an unambiguous atomically precise structure revealed by a single crystal X-ray diffraction (SCXRD) study.[15–20] Chiral metal clusters have constituted an important class of chiral nanomaterials due to their fascinating chiroptical properties.[21–25] Some clusters possess intrinsic chirality in their asymmetric structures and their deracemization has been achieved by employing chiral ligands,[26] chiral HPLC separation[27] and spontaneous resolution.[28,29] Recent works have focused on the dynamic control of chirality in intrinsically chiral metal clusters through ligand engineering.[30–32]

The icosahedral Au_{13} structure is one of the commonly observed superatomic fundamental units in which 12 gold atoms occupy the vertices of the icosahedron and one remaining gold is situated in the center. While the stable icosahedral Au_{13} superatom alone is achiral and highly symmetric, the

Department of Chemistry, Graduate School of Science, Osaka Metropolitan University, 3-3-138 Sugimoto, Sumiyoshi, Osaka 558-8585, Japan.
E-mail: takuya.nakashima@omu.ac.jp

†Electronic supplementary information (ESI) available: Experimental details and supplemental simulation and spectral data. See DOI: https://doi.org/10.1039/d4nr03810j

intrinsic chirality or chiral distortion can be induced mostly by the coordination of bidentate ligands such as bis(diphenylphosphino)ethane (DPPE, Fig. 1).[33,34] The detailed investigation on the crystal structure of the $[Au_{13}(DPPE)_5Cl_2]^{3+}$ cluster demonstrated the distortion between the two gold pentagons (blue and red in Fig. 1 bottom) arranging five bridging DPPE ligands in a helical propeller pattern, indicating the existence of intrinsic chirality in the Au_{13} superatom.[34,35] The deracemization of the Au_{13}-based cluster has been demonstrated by the enantioselective synthesis with chiral ligands,[36–40] spontaneous resolution[41] and enantioseparation with a chiral column.[42] It is of interest to note that the heteroatom doping[41,43] in the center of Au_{13} with Ir^{3+} successfully leads to the spontaneous resolution of the $[IrAu_{12}(DPPE)_5Cl_2]^{+}$ cluster suppressing the rapid racemization upon crystallization. Given the inherent energy barrier for the racemization of the $[Au_{13}(DPPE)_5Cl_2]^{3+}$ cluster is not so small, a slight chiral input may enhance the activation energy biasing the formation of the Au_{13} cluster with a unidirectional twist. In this study, we investigate the effect of the coordination of a chiral ligand on the chirality induction in the Au_{13} superatom cluster. We prepared Au_{13} clusters by using a mixed ligand system of achiral DPPE and chiral (*R*,*R*)-1,2-bis[(2-methoxyphenyl)phenylphosphino]-ethane (*R*-DIPAMP)[36] with a changing DPPE/*R*-DIPAMP (A/C) ratio (Fig. 1). The as-prepared samples displayed optical activity depending on the A/C ratio, while they were composed of a mixture of Au_{13} clusters with different ligand compositions ($[Au_{13}(R\text{-DIPAMP})_x(DPPE)_{5-x}Cl_2]^{3+}$, x = 0–5). The as-prepared samples were therefore separated by means of reverse phase HPLC depending on the x-value. Circular dichroism (CD) measurement for the fractionalized eluents clearly suggested the non-additive effect of the chiral ligand on the chirality induction, demonstrating the "sergeants-and-soldiers principle" in the synthesis of metal clusters for the first time. The entire twist in the Au_{13} superatom is dictated by a single DIPAMP ligand in the $[Au_{13}(R\text{-DIPAMP})_1(DPPE)_4Cl_2]^{3+}$ cluster. The twist in Au_{13} propagates to the helical torsion and arrangement of other four DPPE ligands.

Results and discussion

DFT calculations for Au_{13} clusters protected by DPPE and *R*-DIPAMP ligands ($[Au_{13}(R\text{-DIPAMP})_x(DPPE)_{5-x}Cl_2]^{3+}$, called ***R*0–*R*5**: x = 0–5, respectively) were first carried out to predict the geometries with left- and right-hand twists and their stabilities. Fig. 2 shows the energy diagrams of the P- and M-$[Au_{13}(R\text{-DIPAMP})_x(DPPE)_{5-x}Cl_2]^{3+}$ clusters for the right- and left-hand twisted structures (Fig. 1), respectively. The chiral arrangement of the ligands results in chiroptical properties originating from the helical right- and left-hand structures (global chirality) of Au_{13} clusters.[34,36] It should be noted that the calculation based on the $[Au_{13}(PMe_2Ph)_{10}Cl_2]^{3+}$ structure resulted in an achiral Au_{13} superatom core (θ_2/θ_1 = 1, Fig. 2).[34] The chiral distortion is therefore introduced by the bridging nature of DPPE coordination with a certain P–P distance. When the Au_{13} superatom core is protected by the DPPE ligand, the energy difference between P- and M-Au_{13} clusters is zero because they are enantiomers to each other (Fig. 2). The enantioseparation of them with a chiral column was reported to be unsuccessful probably due to the rapid racemization.[35] In contrast, the protection by *R*-DIPAMP ligands gives diastereomeric isomers with different energies between P- and M-clusters. The DFT calculations for ***R*0–*R*5** reveal that the M-type conformation is destabilized by increasing the number of chiral ligands. While ***R*2** and ***R*3** should have two structural isomers in terms of ligand sequence for each, these isomers were estimated to have negligible energy difference (~0.2 kJ

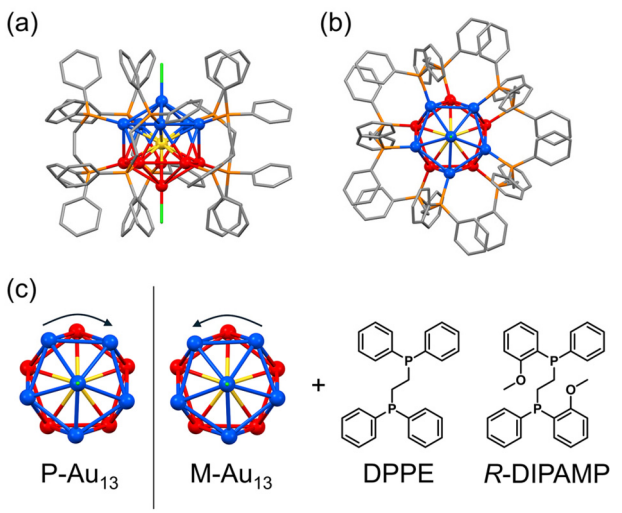

Fig. 1 Structural models of (a and b) $[Au_{13}(DPPE)_5Cl_5]^{3+}$ cluster, and (c) the top views of right- and left-handed helically distorted Au_{13} cores and chemical structures of achiral (DPPE) and chiral (*R*-DIPAMP) ligands discussed in this study.

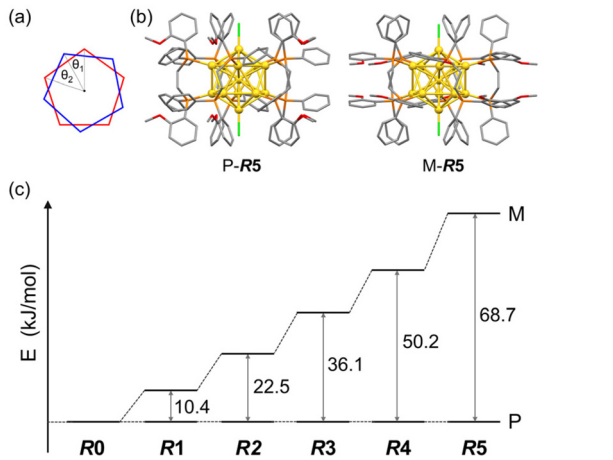

Fig. 2 (a) The torsion angles between the two equatorial Au_5 pentagons in Fig. 1c. (b) The optimized structures of P- and M-$[Au_{13}(R\text{-DIPAMP})_5Cl_2]^{3+}$ clusters by DFT calculation. (c) The energy differences between the P- and M-Au_{13} clusters for ***R*0–*R*5**.

Table 1 The equilibrium constants for the twist inversion between P- and M-***R*1–*R*5** (K = [M-]/[P-***R*1–*R*5**]) and the averaged torsion angles in P-***R*1–*R*5**, estimated by DFT calculations

	***R*1**	***R*2**	***R*3**	***R*4**	***R*5**
K	1.48×10^{-2}	1.15×10^{-4}	4.69×10^{-7}	1.56×10^{-9}	9.12×10^{-13}
θ_2/θ_1	1.200	1.207	1.212	1.217	1.220

mol^{-1}, Fig. S1†). The ratio of averaged torsion angles (θ_2/θ_1) between the two Au-pentagons (Fig. 2a) slightly increases in the order of ***R*1–*R*5** (Table 1), whereas the differences are negligible (<2%) compared to the differences in the energy. The optimized structures for P- and M-conformations of ***R*5** (Fig. 2b) show the distinctive different arrangement of methoxy groups in *R*-DIPAMPs on the exterior shell. The methoxy groups are present in the latitudinal direction of the clusters in P-Au_{13}, whereas, in M-Au_{13}, they are located in the equatorial plane of the clusters, leading to a more crowded stereostructure. This conformational difference in *R*-DIPAMP can be considered as the primary origin of the pronounced energy differences between P-Au_{13} and M-Au_{13}.

The DFT-optimized structures for P-Au_{13} and M-Au_{13} also disclosed the characteristic conformational differences in the diphosphine ligands. The diphosphine ligands coordinate on the surface by tilting to the right (P-***R*1**) or left (M-***R*1**) with respect to the central axis of the icosahedron (Cl–Cl axis), determining the global chirality of Au_{13} clusters. Fig. 3 shows the Newman projections along the ethylene C–C axis for DPPE and *R*-DIPAMP ligands in ***R*1**. The entire ethylene unit adopts an eclipsed conformation, rather than a staggered one. The dihedral angles between the two H–C bonds (φ, Fig. 3) are calculated to be *ca.* +4° (clockwise) for DPPE and *R*-DIPAMP in the stable P-***R*1**, indicating that DPPE and *R*-DIPAMP coordinate to the Au_{13} core with similar geometries regardless of the presence of methoxy groups in P-***R*1**. In contrast, the difference in the conformation of the ethylene unit was observed in M-***R*1**. While the ethylene units of DPPE in M-***R*1** have a mirror-image form of those in P-***R*1** (anticlockwise, φ ~−4°), that of *R*-DIPAMP keeps the clockwise direction (φ ~+5.6°). A similar tendency of the coordination of *R*-DIMPAMP is also confirmed in the optimized structure of P- and M-***R*5**. This result suggests that the *R*-DIPAMP ligand prefers clockwise conformation (in terms of φ) against the global chirality of M-Au_{13}. Thus, a single *R*-DIPAMP ligand plays the role of "sergeant" transferring its chiral coordination structure to other four DPPE on the surface of Au_{13} in P-***R*1** while its role is invalid in M-***R*1**.

Given that the P- and M-Au_{13} isomers are assumed to be in equilibrium, the equilibrium constants (K) for ***R*1–*R*5** at 298 K can be estimated approximating the calculated energy differences as ΔG (Table 1). The population ratio of unstable M-***R*1** at 298 K was calculated to be 1.46% and that for the other ***R*2–*R*5** was approximately zero. While the activation barrier of twist inversion could not be calculated easily, the estimated energy difference suggests that the formation of the P-Au_{13} cluster can be significantly biased by the introduction of just one *R*-DIPAMP ligand.

The synthesis of a series of ***R*0–*R*5** clusters was performed through a previously reported method by changing the ratio of the gold complexes, Au_2(DPPE)Cl_2/Au_2(*R*-DIPAMP)Cl_2, Achiral/Chiral (A/C) ratios = 5/0, 4/1, 3/2, 2/3, 1/4 and 0/5, in the reduction step with $NaBH_4$.[33,36] The reduction of the mixed solution of gold complexes, followed by acid (HCl) etching yielded a mixture of Au_{13} clusters at room temperature. The as-prepared samples were treated by reverse phase column chromatography (Wakosil 100C18, Wako-Fuji Film) using a methanol solution containing 0.5 vol% trifluoroacetic acid (TFA) and 0.5 vol% diethylamine (DEA) as an eluent to remove larger agglomerates. The treated samples afforded almost identical absorption spectra indicating the successful formation of Au_{13} clusters regardless of the A/C ratio (Fig. S2†). Meanwhile, they exhibited optical activity dependent on the A/C ratio for the preparation condition. The A/C = 5/0 and 0/5 samples exclusively contain ***R*0** and ***R*5** with no and the largest optical activity, respectively, while other ratios should give the mixtures of ***R*0–*R*5**. To compare the optical activity, CD spectra were translated to *g*-spectra ($g = \Delta\varepsilon/\varepsilon$) with the equation of g = CD[mdeg]/(32 980·Abs) (Fig. 4a). The plot of anisotropy value (*g*-value) at 550 nm clearly demonstrated the dependence of optical activity on the A/C ratio for the preparative condition. The non-linear relationship between the *g*-value and C/(A + C) ratio suggested the emergence of chiral amplification or the non-additive effect of the chiral ligand on the entire optical activity of Au_{13} clusters. However, the unseparated samples contain ***R*0–*R*5** clusters with a certain distribution. The ESI-MS spectrum for the A/C = 1/4 sample indeed demonstrated that

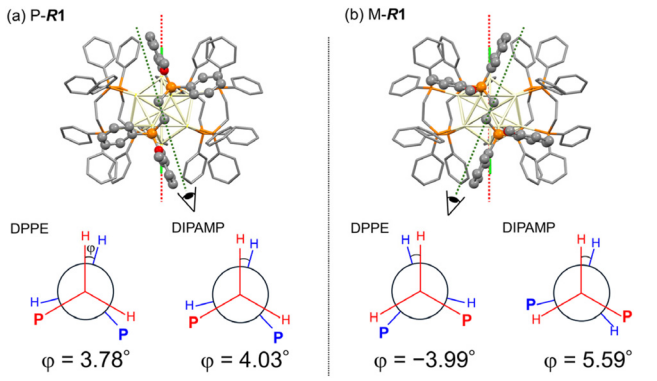

Fig. 3 The optimized structures and Newman projections along the ethylene C–C axis for DPPE and *R*-DIPAMP ligands of (a) P-***R*1** and (b) M-***R*1**. *R*-DIPAMP ligands are highlighted with a ball and stick model. The dihedral angle for the DPPE ligand was calculated as an averaged value of four DPPE ligands.

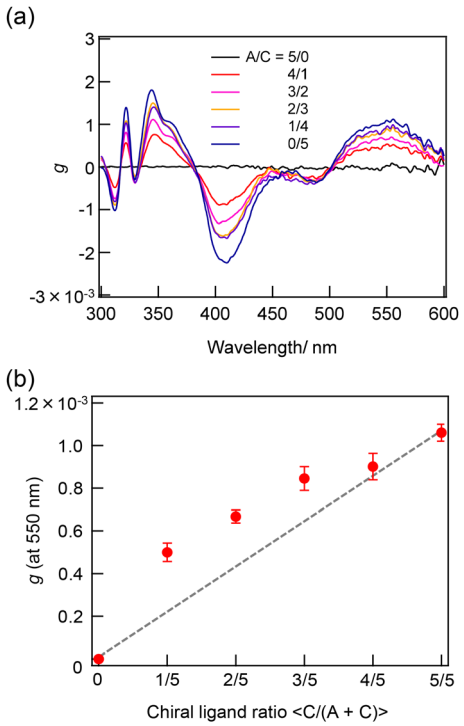

Fig. 4 (a) *g*-Spectra of the sample prepared with A/C = 5/0–0/5 ratios and (b) the plot of *g*-values at 550 nm as a function of C/(A + C) ratio in the synthetic condition.

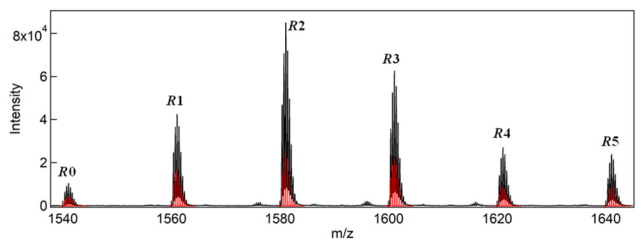

Fig. 5 ESI-MS spectrum of the sample prepared with A/C = 1/4 ratio together with simulated isotope peak patterns (red bars) for ***R*0–*R*5**.

the solution contains all possible compositions (Fig. 5). Furthermore, the result of DFT calculation motivated us to isolate ***R*0–*R*5** species to investigate the effect of single chiral ligand coordination on the optical activity of Au_{13} clusters.

Negishi and coworkers demonstrated the precise HPLC separation of nonionic $PdAu_{24}(SR)_{18-n}(SR')_n$ clusters by gradient elution using a reverse phase column.[44,45] On the other hand, a tricationic $[Au_{13}(bisNHC)_5Cl_2]^{3+}$ (NHC: N-heterocyclic carbene) cluster was subjected to a chiral column using methanol as an eluent with TFA/DEA additives.[42] In the present study, a preparative reverse phase column (InertSustain C30, GL Science) was employed and a gradient elution condition was considered. Finally, the successful separation was achieved by using the mixture of methanol containing TFA (0.2 vol%) and DEA (0.2 vol%) and water (see the ESI† for details). Fig. 6 shows the result of the HPLC separation. The A/C = 5/0 sample

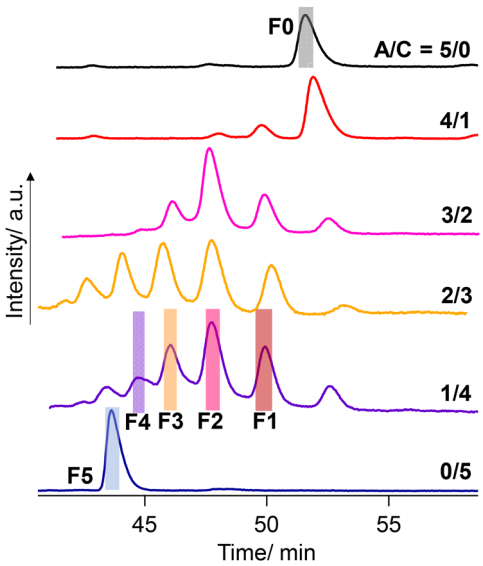

Fig. 6 HPLC chromatograms for the mixture solutions of $[Au_{13}(R\text{-DIPAMP})_x(DPPE)_{5-x}Cl_2]^{3+}$ clusters synthesized with different A/C ratios.

gave a single peak at 52–53 min collected as **F0** (fraction 0, Fig. 6), which was confirmed as the ***R*0** cluster with ESI-MS (Fig. S3†). Meanwhile, the A/C = 0/5 sample afforded a peak at the shorter retention time assigned to ***R*5**, which was collected as **F5**. The retention times in the HPLC charts for A/C = 4/1–1/4 samples were adjusted by using ***R*0** peaks as a standard. The A/C = 1/4 sample, ESI-MS data of which demonstrated the presence of all species ***R*0–*R*5** (Fig. 5), displayed 4 more peaks in-between the peaks assigned to ***R*0** and ***R*5**, indicating the separation of all the species. To confirm the separation of ***R*1–*R*4**, the eluate was fractionalized into **F1–F4** depending on the peak positions (Fig. 6). The ESI-MS measurement demonstrated that **F1–F4** exclusively contain ***R*1–*R*4**, respectively (Fig. S3†). While two isomers with different ligand sequences for ***R*2** and ***R*3** could not be discriminated, successful separation was achieved in terms of ligand compositions.

The peak intensity ratio in the ESI-MS spectrum for the A/C = 1/4 sample (Fig. 5) well accorded with that in the elution profile (Fig. 6) corresponding to the abundance ratio of ***R*0–*R*5**. However, this distribution was far different from the theoretical one assuming the random incorporation of the ligand based on the given A/C ratio (Fig. S4†). The A/C = 1/4 ratio should give ***R*4** and ***R*5** as the major and second major products with 45 and 30% probabilities and there is a negligible chance for the ***R*0** formation. The experimental result suggests the less reactivity of the DIPAMP ligand for the coordination on the Au_{13} cluster than DPPE. The A/C = 4/1 condition highlights the less reactivity of DIPAMP by the formation of ***R*0** as the major product with faint formation of ***R*1** and ***R*2** (Fig. 6). The two-step reaction mechanism for the efficient synthesis of Au_{13} clusters has been discussed by Shichibu and Konishi.[33] The first reduction process of Au_2(diphosphine)Cl_2 gives a mixture of polydispersed gold clusters with various compositions. These polydispersed clusters converged to

$[Au_{13}(diphosphine)_5Cl_2]^{3+}$ upon the addition of HCl aq. Most of the kinetically formed metastable clusters were subjected to etching being consumed as precursors forming the most stable one. While both the enantiomers of $[Au_{13}(DPPE)_5Cl_2]^{3+}$ have identical stability, the M-Au_{13} clusters containing *R*-DIPAMP ligands should have less stability than P-ones (Fig. 2), being subject to etching. Furthermore, achiral DPPE is considered to preferentially participate in the coordination on the preformed M-Au_{13} superatom over *R*-DIPAMP with adopting the torsional conformation appropriate for the left-hand twisted cluster (Fig. 3). The formation of ***R*0** thus preferentially proceeds in the condition of a small chiral ligand content.

When the content of chiral ligand changed from A/C = 4/1 to 3/2, the major product drastically changed from ***R*0** to ***R*2**. While the incorporation of *R*-DIPAMP in the Au_{13} cluster formation seems less probable than DPPE, the yield of ***R*2** is higher than that of ***R*1**. The coordination of the first *R*-DIPAMP ligand might facilitate the introduction of the second *R*-DIPAMP in a similar manner to the emergence of the allosteric effect in the chiral guest incorporation by prochiral double decker porphyrins.[46,47] More specifically, if an Au_{13} superatom with P-type twist induced by the single *R*-DIPAMP coordination had a vacant coordination site, *R*-DIPAMP with a geometry preorganized (Fig. 3) for the coordination on the P-type cluster could be more feasible than DPPE to fill that site. However, the inherent less reactivity with sterically less flexible nature compared to DPPE may result in the less formation probabilities of ***R*3**, ***R*4** and ***R*5** for the conditions of A/C = 3/2, 2/3 and 1/4. Another possibility includes the selective consumption of the chiral DIPAMP ligand for the formation of cluster species other than Au_{13}, resulting in the decrease of practical chiral ligand ratio to form Au_{13} clusters.

The absorption and CD measurements were carried out for the fractions of **F1–F5**. As described above, the ESI-MS measurement for **F1–F5** demonstrated the successful isolation of Au_{13} clusters into a single composition of ***R*1–*R*5**, respectively. At the very least, no trace of ***R*0** was contained in those fractions because of its well-separated peak position in the HPLC charts (Fig. 6). All **F1–F5** fractions containing ***R*1–*R*5**, respectively, exhibited almost identical absorption and CD profiles (Fig. S5 and S6†). Furthermore, the *g*-spectra of ***R*1–*R*4** showed similar profiles to that of ***R*5** with very similar *g*-values at 550 nm (Fig. 7). The contamination of ***R*0** in the solutions should result in a lower optical activity of the unseparated samples than that of ***R*5** (Fig. 4). The result thus confirmed that the single coordination of the *R*-DIPAMP ligand is enough to induce a unidirectional helical twist in the Au_{13} superatom as predicted by the DFT study. Meanwhile, other four achiral DPPE ligands adopt the helical torsional conformation following the one-hand twist in the Au_{13} superatom (Fig. 3).

Bürgi and coworkers have extensively utilized the HPLC technique to monitor the ligand exchange reaction of the intrinsically chiral $Au_{38}(SR)_{24}$ clusters and to isolate the ligand-exchanged products.[30,48–51] The intrinsically chiral Au_{38} enantiomer demonstrated the diastereoselective ligand exchange with chiral ligands, suppression of racemization by

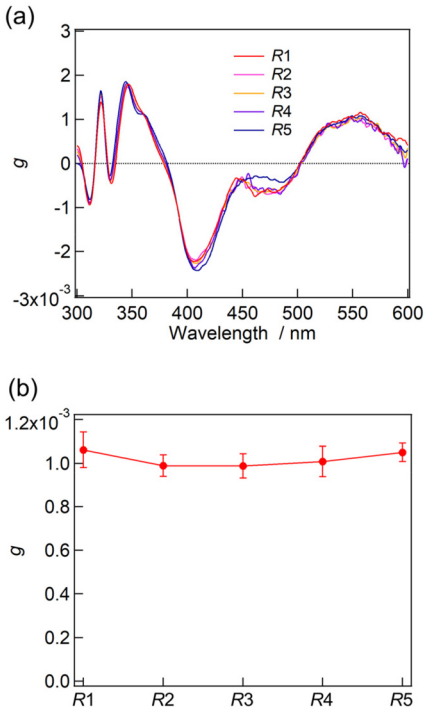

Fig. 7 (a) *g*-Spectra of ***R*1–*R*5** separated by HPLC. (b) The plot of *g*-values at 550 nm for ***R*1–*R*5**.

the introduction of a chiral ligand and modulation of optical activity by the ligand exchange. In the present study, the HPLC separation of chiral–achiral mixed-ligand-protected clusters disclosed the clear composition–chiroptical property relationship with a one-to-one correspondence.

The CD spectra of ***R*1–*R*5** were well reproduced by DFT calculations (Fig. S7†). While the compositions in the ligand shell are different, ***R*1–*R*5** gave very similar CD spectra which also supports that the first Cotton effect originates from the internal chirality in the helical superatom core (Au_{13}). The average torsion angles calculated from the optimized structures of ***R*1–*R*5** slightly increased by increasing the number of *R*-DIPAMP as discussed above (Table 1). Although the nearly similar torsion angles of ***R*1–*R*5** may have minimal effect on the intensity of the CD signal, these experimental results support the argument that the chiroptical properties arise from the differences in the angle between the two Au-pentagons.[34]

Conclusion

The effect of a chiral ligand on the chirality induction in $[Au_{13}(diphosphine)_5Cl_2]^{3+}$ clusters has been investigated. The DFT calculation indicated that the coordination of the single chiral ligand DIPAMP could greatly stabilize the one-handed twist structure in an icosahedral Au_{13} superatom core with 98.5% occupancy over the opposite-twist regardless of the presence of other four achiral DPPE ligands. While the synthesis in a mixed ligand system of DPPE and *R*-DIPAMP led to the for-

mation of a mixture of $[Au_{13}(R\text{-DIPAMP})_x(DPPE)_{5-x}Cl_2]^{3+}$ clusters, they have been successfully separated into individual compositions in terms of x-values (x = 0–5) by reverse-phase HPLC. The fractionalized HPLC eluents including ***R*1–*R*5**, free from $[Au_{13}(DPPE)_5Cl_2]^{3+}$ (***R*0**), afforded identical optical activity clearly supporting the result of DFT calculation. Thus the non-additive effect of the chiral ligand on the chirality induction in the Au_{13} cluster has been demonstrated in theoretical and experimental manners. In other words, the chirality of the DIPAMP ligand could be successfully communicated into a chiral conformation of DPPE.[52] The HPLC separation technique[53,54] should provide the opportunity of clear role division between different ligands for mixed-ligand clusters, further expanding the usage of ligands as toolboxes in functional clusters.[55]

Author contributions

K. M.: investigation, funding acquisition, visualization, writing – original draft, and writing – review & editing. S. K.: investigation. T. Y.: investigation. T. N.: conceptualization, investigation, funding acquisition, resources, supervision, and writing – review & editing.

Data availability

The data supporting this article have been included as part of the ESI.†

Conflicts of interest

There are no conflicts to declare.

Acknowledgements

This work was financially supported by JST CREST (Grant Number: JPMJCR20B2), JSPS KAKENHI grant numbers JP22H05134 (TN) for Transformative Research (A) "Revolution of Chiral Materials Science using Helical Light", JP23H01938 (TN) and JP24K01458 (KM) for Scientific Research (B), and by Tokyo Ohka Foundation for The Promotion of Science and Technology for K. M. A part of this work was conducted in the Institute for Molecular Science, supported by "Advanced Research Infrastructure for Materials and Nanotechnology in Japan (ARIM)" of the Ministry of Education, Culture, Sports, Science and Technology (MEXT). Proposal Number JPMXP1224MS0001.

References

1 R. Noyori and M. Kitamura, *Angew. Chem., Int. Ed. Engl.*, 1991, **30**, 49–69.
2 H. B. Kagan, *Synlett*, 2001, 888–899.
3 T. Satyanarayana, S. Abraham and H. B. Kagan, *Angew. Chem., Int. Ed.*, 2009, **48**, 456–494.
4 S. Sioncke, T. Verbiest and A. Persoons, *Mater. Sci. Eng., R*, 2003, **42**, 115–155.
5 X. Yan, Q. Wang, X. Chen and Y.-B. Jiang, *Adv. Mater.*, 2020, **32**, 1905667.
6 M. Rok, A. Miniewicz, M. Zdończyk, B. Zarychta, J. W. Mikurenda, S. Bartkiewicz, M. Wiśniewska-Bełej, J. Cybińska and A. Piecha-Bisiorek, *J. Phys. Chem. Lett.*, 2024, **15**, 5276–5287.
7 J. S. Siegel, *Chirality*, 1998, **10**, 24–27.
8 D. G. Blackmond and M. Klussmann, *Chem. Commun.*, 2007, 3990–3996.
9 K. K. Konstantinov and A. F. Konstantinova, *Origins Life Evol. Biospheres*, 2018, **48**, 93–122.
10 N. Suzuki and Y. Itabashi, *Symmetry*, 2019, **11**, 966.
11 A. R. A. Palmans and E. W. Meijer, *Angew. Chem., Int. Ed.*, 2007, **46**, 8948–8968.
12 E. Yashima, N. Ousaka, D. Taura, K. Shimomura, T. Ikai and K. Maeda, *Chem. Rev.*, 2016, **116**, 13752–13990.
13 M. M. Green and P. Ridy, *J. Am. Chem. Soc.*, 1989, **111**, 6452–6454.
14 A. R. A. Palmans, J. A. J. M. Vekemans, E. E. Havinga and E. W. Meijer, *Angew. Chem., Int. Ed. Engl.*, 1997, **36**, 2648–2651.
15 R. Jin, C. Zeng, M. Zhou and Y. Chen, *Chem. Rev.*, 2016, **116**, 10346–10413.
16 Y. Du, H. Sheng, D. Astruc and M. Zhu, *Chem. Rev.*, 2020, **120**, 526–622.
17 S. Takano and T. Tsukuda, *J. Am. Chem. Soc.*, 2021, **143**, 1683–1698.
18 Y. Saito, C. Murata, M. Sugiuchi, Y. Shichibu and K. Konishi, *Coord. Chem. Rev.*, 2022, **470**, 214713.
19 W. Du, S. Jin, L. Xiong, M. Chen, J. Zhang, X. Zou, Y. Pei, S. Wang and M. Zhu, *J. Am. Chem. Soc.*, 2017, **139**, 1618–1624.
20 S. Chen, S. Wang, J. Zhong, Y. Song, J. Zhang, H. Sheng, Y. Pei and M. Zhu, *Angew. Chem., Int. Ed.*, 2015, **54**, 3145–3149.
21 Y. Li, T. Higaki, X. Du and R. Jin, *Adv. Mater.*, 2020, **32**, e1905488.
22 Y. Zhu, J. Guo, X. Qiu, S. Zhao and Z. Tang, *Acc. Mater. Res.*, 2020, **2**, 21–35.
23 Y. Shichibu and K. Konishi, *ChemNanoMat*, 2022, **8**, e202200194.
24 J.-H. Huang, X.-Y. Dong, Y.-J. Wang and S.-Q. Zang, *Coord. Chem. Rev.*, 2022, **470**, 214729.
25 K. K. Ramankutty, *Nanoscale*, 2024, **16**, 11914–11927.
26 J. Kumar, T. Kawai and T. Nakashima, *Chem. Commun.*, 2017, **53**, 1269–1272.
27 I. Dolamic, S. Knoppe, A. Dass and T. Bürgi, *Nat. Commun.*, 2012, **3**, 798.
28 J. H. Huang, Z. Y. Wang, S.-Q. Zang and T. C. W. Mak, *ACS Cent. Sci.*, 2020, **6**, 1971–1976.
29 S. Chen, W. Du, C. Qin, D. Liu, L. Tang, Y. Liu, S. Wang and M. Zhu, *Angew. Chem., Int. Ed.*, 2020, **59**, 7542–7547.

30 Y. Wang, B. Nieto-Ortega and T. Bürgi, *Nat. Commun.*, 2020, **11**, 4562.
31 H. Yoshida, M. Kuzuhara, R. Tanibe, T. Kawai and T. Nakashima, *J. Phys. Chem. C*, 2021, **125**, 27009–27015.
32 T. Nakashima, R. Tanibe, H. Yoshida, M. Ehara, M. Kuzuhara and T. Nakashima, *Angew. Chem., Int. Ed.*, 2022, **61**, e202208273.
33 Y. Shichibu and K. Konishi, *Small*, 2010, **6**, 1216–1220.
34 Y. Shichibu, Y. Ogawa, M. Sugiuchi and K. Konishi, *Nanoscale Adv.*, 2021, **3**, 1005–1011.
35 J. Zhang, Y. Zhou, K. Zheng, H. Abroshan, D. R. Kauffman, J. Sun and G. Li, *Nano Res.*, 2018, **11**, 5787–5798.
36 Y. Yang, Q. Zhang, Z.-J. Guan, Z.-A. Nan, J.-Q. Wang, T. Jia and W.-W. Zhan, *Inorg. Chem.*, 2019, **58**, 3670–3675.
37 P. Luo, X.-J. Zhai, S. Bai, Y.-B. Si, X.-Y. Dong, Y.-F. Han and S.-Q. Zang, *Angew. Chem., Int. Ed.*, 2023, **62**, e202219017.
38 H. Hirai, T. Nakashima, S. Takano, Y. Shichibu, K. Konishi, T. Kawai and T. Tsukuda, *J. Mater. Chem.*, 2023, **11**, 3095–3100.
39 Y. Sato, M. Mitani and H. Yao, *J. Phys. Chem. C*, 2020, **124**, 25547–25556.
40 E. L. Albright, S. Malola, S. I. Jacob, H. Yi, S. Takano, K. Mimura, T. Tsukuda, H. Häkkinen, M. Nambo and C. M. Crudden, *Chem. Mater.*, 2024, **36**, 1279–1289.
41 H. Hirai, S. Takano, T. Nakamura and T. Tsukuda, *Inorg. Chem.*, 2020, **59**, 17889–17895.
42 H. Yi, K. M. Osten, T. I. Levchenko, A. J. Veinot, Y. Aramaki, T. Ooi, M. Nambo and C. M. Crudden, *Chem. Sci.*, 2021, **12**, 10436–10440.
43 H. Hirai, S. Takano, T. Nakashima, T. Iwasa, T. Taketsugu and T. Tsukuda, *Angew. Chem., Int. Ed.*, 2022, **61**, e202207290.
44 Y. Niihori, M. Matsuzaki, T. Pradeep and Y. Negishi, *J. Am. Chem. Soc.*, 2013, **135**, 4946–4949.
45 Y. Niihori, M. Matsuzaki, C. Uchida and Y. Negishi, *Nanoscale*, 2014, **6**, 7889–7896.
46 S. Shinkai, M. Ikeda, A. Sugasaki and M. Takeuchi, *Acc. Chem. Res.*, 2001, **34**, 494–503.
47 T. Ikeda, K. Sada, S. Shinkai and M. Takechi, *Supramol. Chem.*, 2011, **23**, 59–64.
48 S. Knoppe, R. Azoulay, A. Dass and T. Bürgi, *J. Am. Chem. Soc.*, 2012, **134**, 20302–20305.
49 S. Knoppe, S. Michalet and T. Bürgi, *J. Phys. Chem. C*, 2013, **117**, 15354–15361.
50 A. Baghdasaryan, K. Martin, L. M. L. Daku, M. M. Talamo, N. Avarvari and T. Bürgi, *Nanoscale*, 2020, **12**, 18160–18170.
51 Y. Wang, Ee. Makkonen, X. Chen and T. Bürgi, *Chem. Sci.*, 2021, **12**, 9413–9419.
52 I. Dolamic, B. Varnholt and T. Bürgi, *Nat. Commun.*, 2015, **6**, 7117.
53 Y. Niihori, C. Uchida, W. Kurashige and Y. Negishi, *Phys. Chem. Chem. Phys.*, 2016, **18**, 4251–4265.
54 Y. Niihori, D. Shima, K. Yoshida, K. Hamada, L. V. Nair, S. Hossain, W. Kurashige and Y. Negishi, *Nanoscale*, 2018, **10**, 1641–1649.
55 K. Konishi, M. Iwasaki, M. Sugiuchi and Y. Shichibu, *J. Phys. Chem. Lett.*, 2016, **7**, 4267–4274.